

Non-isothermal crystallization kinetic and compatibility of PTT/PP blends by using maleic anhydride grafted polypropylene as compatibilizer

Yingjin Wang · Mingtao Run

Received: 19 November 2008 / Accepted: 20 February 2009 / Published online: 18 March 2009
© Springer Science + Business Media B.V. 2009

Abstract The crystallization behaviors, non-isothermal crystallization kinetics, and the morphology of poly(trimethylene terephthalate)/Polypropylene (PTT/PP) blends using a maleic anhydride grafted polypropylene (PP-g-MAH) as a compatibilizer were investigated by differential scanning calorimeter (DSC) and scanning electron microscope (SEM), respectively. The results suggested that the blends exhibited different crystallization and melting behaviors due to different content of PP-g-MAH. All of the DSC curves of the blends exhibited two exothermic peaks and endothermic peaks. The commonly used Avrami equation modified by Jeziorny, Ozawa theory and the method developed by Mo were used, respectively, to fit the primary stage of non-isothermal crystallization process. The results suggested that the crystallization rate of PTT component was increased, whereas, that of PP component was retarded with the introduction of PP-g-MAH. The effective activation energy was calculated by differential iso-conversional method developed by Vyazovkin. The SEM result suggested that the introduction of PP-g-MAH greatly improved the compatibility between PTT and PP, and decreased the size of dispersed particles.

Keywords Poly(trimethylene terephthalate) · Polypropylene · Non-isothermal crystallization kinetic · Compatibility

Y. Wang (✉)
Lab of Biochemical Analysis, Xinzhou Teacher's University,
Xinzhou 034000, China
e-mail: yingjinyaya@hotmail.com

M. Run
College of Chemistry & Environmental Science,
Hebei University,
Baoding 071002, China

Introduction

Poly(trimethylene terephthalate) (PTT) was first patented by Whinfield and Dickson [1] in 1941. Many properties of PTT are between those of poly(ethylene terephthalate) (PET) and poly(butylene terephthalate) (PBT), such as crystallization rate and mechanical property. Moreover, it combines the key advantages of PET and PBT into one polymer and has an important application in textile industry [2] and engineering thermoplastic [3]. Polypropylene (PP) is a well-established high volume commodity polymer, which has a comprehensive application in many fields such as home appliances, automotive and construction. In the last decades, remarkable studies about PP [4–11], blends of PP with other polymers have been reported [12–20].

Polymer blending is an attractive alternative for producing new polymeric materials with desirable properties without synthesizing a totally new material. Other advantages for polymer blending are versatility, simplicity, and inexpensiveness. Due to the important application of the two polymers, numerous research works related to various aspects of the two polymers are available in the reported literatures [21–26]. In general, melt mixing of two polymers result in a two-phase system because polymers are often thermodynamically immiscible, which further lead to a high interfacial tension and poor interphase adhesion. Interfacial tension leads to the desired degree of dispersion of random mixtures, and the poor adhesion contributes to weak and brittle mechanical properties. For PTT/PP blend, these two polymers are not miscible or compatible because they have a large difference in their solubility parameters since they dissolve only in solvents with vastly different polarities. In order to combine the super properties of both polymers and obtain morphological blends which give rise to good mechanical properties in incompatible blends,

compatibilizing agents are necessary to promote interfacial interactions. In our researches, by adding a maleic anhydride grafted polypropylene (PP-g-MAH), the compatibility between PTT and PP is enhanced through the reaction between the maleic anhydride moiety and PTT's hydroxyl endgroup during melt blending. This kind of surface activity reduces the interfacial energy between the two phases and improves the interfacial adhesion and produces a finer dispersion mixing.

The study of polymer blend crystallization behavior is important because the process affects the resultant blend super molecular structures, their physical and mechanical properties. However, most of studies on crystallization behavior were focus on amorphous/crystalline blends; the studies on crystalline/crystalline blends [27] are comparatively fewer. In general, crystallization behavior of a two crystalline component blend is more complicated because the presence of one crystalline polymer may accelerate, interfere or even suppress the other polymer's ability to crystallize, depending on the degree of their compatibility, the composition, and the reaction between the component polymers. In this paper, the effects of compatibilizer on the crystallization process, nucleation and growth mechanisms, and compatibility between PTT and PP component in the polypropylene-polyesters blends were systemically investigated.

Theoretical backgrounds

The relative crystallinity ($X_c(t)$) as a function of time is defined as the following equation:

$$X_c(t) = \frac{\int_{t_0}^t (dH_c/dt) dt}{\int_{t_0}^{t_\infty} (dH_c/dt) dt} = \frac{A_0}{A_\infty} \quad (1)$$

where t_0 and t_∞ are the time, at which crystallization starts and ends, and A_0 and A_∞ are areas under the normalized DSC curves. The half time of crystallization ($t_{1/2}$) is the required time for 50% crystallization. Generally, the smaller the value of $t_{1/2}$, the faster the crystallization rate is.

The Avrami theory modified by Jeziorny

The Avrami theory [28] has been widely used for the interpretation of the isothermal crystallization process:

$$1 - X_c(t) = \exp(-Z_t t^n) \quad (2)$$

$$\log[-\ln(1 - X_c(t))] = n \log t + \log Z_t \quad (3)$$

where $X_c(t)$ is the relative degree of crystallinity at time t ; the exponent n is a mechanism constant with a value depending on the type of nucleation and the growth

dimension, and the parameter Z_t is a growth rate constant involving both nucleation and growth rate parameters. The exponent n and Z_t can be obtained from the slope and intercept of the line in the plot.

Although, the physical meanings of Z_t and n cannot be related to the non-isothermal case in a simple way, it can also been used to describe non-isothermal processes [29], and their use provides further insight into the kinetics of non-isothermal crystallization. The crystallization time t can be obtained by the following equation:

$$t_c = \frac{T_s - T}{D} \quad (4)$$

where T is the temperature of crystallization time t_c , T_s is the temperature at which crystallization starts and D is the cooling rate. From the Eqs. 3 and 4, we obtain:

$$\log[-\ln(1 - X_c(t))] = n \log\left(\frac{T_s - T}{D}\right) + \log Z_t \quad (5)$$

Considering the non-isothermal characteristics of the process investigated, the parameters for the value of the crystallization rate, Z_t , should be corrected by the cooling rate D , because the temperature constantly change during the process. The parameter characterizing the kinetics of non-isothermal crystallization was given by Jeziorny as follow:

$$\log Z_c = \frac{\log Z_t}{D} \quad (6)$$

where Z_c is the kinetic crystallization rate constant.

The Ozawa theory [30]

Ozawa extended the Avrami equation to the non-isothermal condition. Assuming that the non-isothermal crystallization process may be composed of infinitesimally small isothermal crystallization steps, the following equation was derived:

$$1 - X_c(T) = \exp\left[-\frac{K(T)}{|D|^m}\right] \quad (7)$$

$$\log[-\ln(1 - X_c(T))] = \log K(T) - m \log D \quad (8)$$

where D is the cooling rate, $K(T)$ is a function related to the overall crystallization rate that indicates how fast crystallization proceeds, and m is the Ozawa exponent that depends on the dimension of crystal growth. According to Ozawa's theory, the relative crystallinity, $X_c(T)$, can be calculated from these equations. By drawing the plot of $\log[-\ln(1 - X_c(T))]$ versus $\log D$ at a given temperature, we should obtain a series of straight lines if the Ozawa analysis is valid, and the kinetic parameters m and $K(T)$ can be derived from the slope and the intercept, respectively.

The theory of Mo [31]

Mo et al. proposed a different kinetic equation by combining the Avrami and Ozawa equations. As the degree of crystallinity was related to the cooling rate D and the crystallization time t (or T), the relationship between D and t could be defined for a given degree of crystallinity. Consequently, a new kinetic equation for non-isothermal crystallization was derived by combining Eqs. 3 and 8:

$$\log Z_t + n \log t = \log K(T) - m \log D \tag{9}$$

$$\log D = \log F(T) - b \log t \tag{10}$$

where the parameters $F(T) = [K(T)/Z_t]^{1/m}$, and b is the ratio between the Avrami and Ozawa exponents, i.e. $b=n/m$. $F(T)$ refers to the value of cooling rate chosen at unit crystallization time when the system amounted to a certain degree of crystallinity. The smaller the value of $F(T)$ is, the higher the crystallization rate becomes. Therefore, $F(T)$ has a definite physical and practical meaning.

Crystallization activation energy

In order to obtain the reliable values of the effective activation energy on the melt cooling process, Friedman [32] and Vyazovkin [33, 34] developed differential iso-conversional method and advanced iso-conversional method, respectively. In this paper, the Vyazovkin analysis is carried out by first differentiating the X_t function with respect to time to obtain the instantaneous crystallization rate as a function of time dX_t/dt . The Vyazovkin equation is express as:

$$\Phi(E_a) = \sum_{i=1}^n \sum_{j \neq i}^n \frac{J[E_a, T_i(t_a)]}{J[E_a, T_j(t_a)]} \tag{11}$$

where

$$J[E_a, T_i(t_a)] \equiv \int_{t_a-\Delta a}^{t_a} \exp\left[\frac{-E_a}{RT_i(t)}\right] dt \tag{12}$$

In Eq. 12, a varies from a to $1-\Delta a$ with a step $\Delta a=m-1$, where m is the number of intervals chosen for analysis and it is set as $m=50$.

Experimental

Materials

The poly(trimethylene terephthalate) (PTT) homopolymer was supplied in pellet form by Shell Chemicals (USA) with

an intrinsic viscosity of 0.92 dL/g measured in a phenol/tetrachloroethane solution (50/50, w/w) at 25 °C. The polypropylene (PP) ($MI_{2.30/2.16}$ is 1.98 g/10 min) was purchased from the Tianjin Petroleum Chemical Plant (China) (the brand was EPS30R). The maleated polypropylene (PP-g-MAH) ($MFI_{230/2.16}$ is 20 g/10 min) with graft efficiency of 0.9 wt.% was prepared by reactive extrusion in Institute of Chemistry Chinese Academy of Science.

Blends preparation

The materials were dried in a vacuum oven at 90 °C for 10 h before preparing blends. The dried pellet of PTT, PP and PP-g-MAH were mixed together with settled weight ratio of PTT/PP=4/1 and the weight ratio of PP-g-MAH as following: B0: 0%, B1: 5%, B2: 10%, B3: 20%, B4: 30%, the pure PP was signed as B5, and the pure PTT was signed as B6. And then melt-blended in a ZSK-25WLE WP self-wiping, co-rotating twin-screw extruder at a screw speed of 60 rpm and a die temperature of 260 °C. The resultant blend ribbons were cooled in cold water, cut up, re-dried before test.

Differential scanning calorimetry (DSC)

The crystallization and subsequent melting behaviors of various binary blends were studied by the Perkin-Elmer Diamond DSC instrument that calibrated with indium prior to performing the measurement; the weights of all samples were approximately 6.0 ± 0.5 mg. The samples were performed as following: The samples were heated to 250 °C at 150 °C/min under a nitrogen atmosphere, held

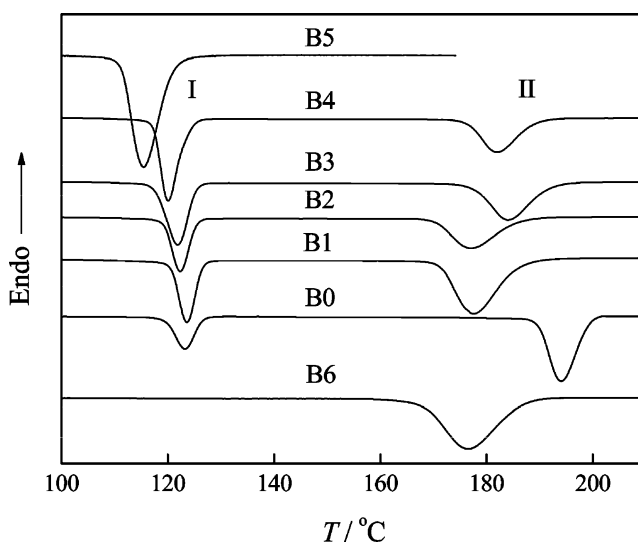


Fig. 1 DSC melt-crystallization curves of seven samples at the cooling rate of 10 °C/min

Table 1 Parameters of seven samples during crystallization and melting process

Sample	PP				PTT			
	$T_{cl}/^{\circ}\text{C}$	$\Delta H_{cl}/\text{J}\cdot\text{g}^{-1}$	$T_{ml}/^{\circ}\text{C}$	$\Delta H_{ml}/\text{J}\cdot\text{g}^{-1}$	$T_{cl}/^{\circ}\text{C}$	$\Delta H_{cl}/\text{J}\cdot\text{g}^{-1}$	$T_{ml}/^{\circ}\text{C}$	$\Delta H_{ml}/\text{J}\cdot\text{g}^{-1}$
B6	–	–	–	–	176.6	–50.5	225.0	–65.9
B0	123.2	–16.8	167.6	–15.5	194.1	–43.8	230.6	–34.6
B1	123.7	–17.8	166.1	–18.1	176.9	–38.7	228.4	–36.8
B2	122.4	–23.7	165.4	–23.8	177.3	–34.2	228.5	–32.6
B3	121.9	–29.8	164.7	–29.3	184.0	–32.7	228.1	–30.9
B4	120.1	–36.5	163.8	–35.6	182.1	–28.1	228.0	–27.7
B5	115.5	–81.1	161.7	–90.0	–	–	–	–

for 5 min and cooled to 50 °C at a constant cooling rate of 10 °C/min, heated again to 250 °C at a rate of 10 °C/min, the cooling process and the second heating process were recorded, respectively.

The non-isothermal crystallization behaviors of two blends (B1 and B4) were performed as following: the sample were heated to 250 °C in nitrogen, held for 5 min and cooled to 50 °C at constant cooling rates of 5, 7.5, 10, 15, 20, 30, 40 °C/min, respectively. The exothermic curves of heat flow as a function of temperature were recorded and investigated.

Scanning electron microscope (SEM)

Travor-Norther KYKY-1000B scanning electron microscope (SEM) instrument was used to observe the blend morphology. The samples were cri-fractured in liquid nitrogen and the fracture surface was coated with gold before examination.

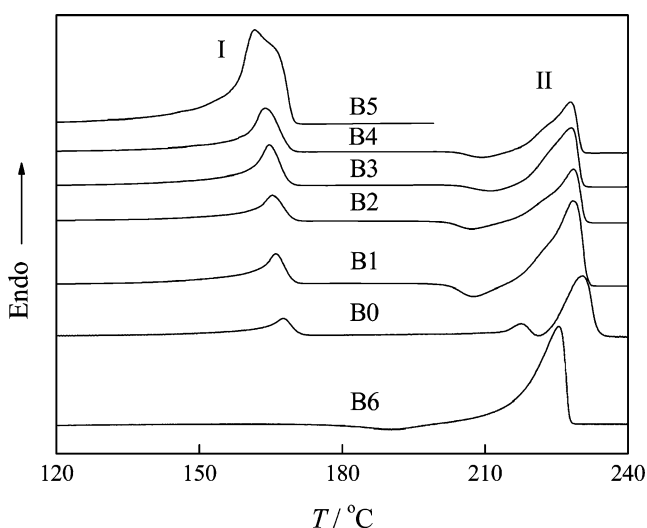
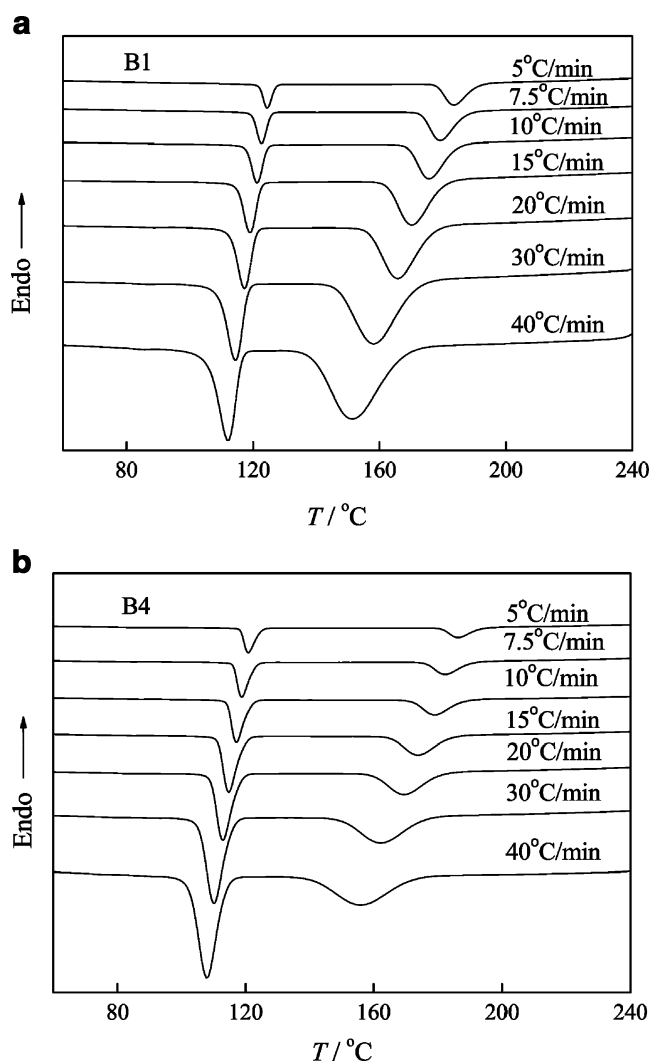
**Fig. 2** DSC melting thermograms of seven samples at the heating rate of 10 °C/min**Fig. 3** Non-isothermal crystallization curves of **a** B1 and **b** B4 blends at different cooling rates

Table 2 Parameters of non-isothermal crystallization analyzed by Avrami theory for PTT component of B1 and B4 blends

Samples	$D/^\circ\text{C}\cdot\text{min}^{-1}$	$T_m/^\circ\text{C}$	$t_{1/2}/\text{s}$	n	$\log Z_c/s^{-n}$	$\log Z_d/s^{-n}$	$\Delta H/\text{J}\cdot\text{g}^{-1}$
B1	5	183.4	210.2	5.9	-13.85	-2.77	-40.4
	7.5	179.3	148.0	5.7	-12.45	-1.66	-39.9
	10	175.7	109.7	5.2	-10.81	-1.08	-38.8
	15	170.4	88.0	5.5	-10.77	-0.72	-38.1
	20	165.8	78.4	5.8	-11.06	-0.55	-37.6
	30	158.3	58.2	5.3	-9.54	-0.32	-36.6
	40	151.5	46.9	4.9	-8.38	-0.21	-36.1
B4	5	186.5	178.7	5.7	-11.52	-2.30	-29.3
	7.5	182.7	133.5	4.9	-10.77	-1.44	-28.6
	10	179.1	124.7	4.8	-12.29	-1.23	-28.4
	15	173.8	79.6	5.4	-9.28	-0.62	-27.7
	20	169.6	71.6	4.7	-9.68	-0.48	-27.4
	30	162.2	56.0	5.0	-8.81	-0.29	-26.8
	40	155.6	43.0	5.3	-7.08	-0.18	-26.3

Results and discussion

Melt-crystallization and subsequent melting behavior

Figure 1 shows the DSC curves of seven samples at a given cooling rate of 10 °C/min, and the crystallization parameters are listed in Table 1. According to Fig. 1 and Table 1, an apparent exotherm is observed for B5 (pure PP) and B6 (pure PTT) samples at 115.5 and 176.6 °C, respectively. However, the exotherms from B0 to B4 blends exhibit two main crystallization peaks: the peak II (T_{cII}) at higher temperature and peak I (T_{cI}) at lower temperature, which may be attributed to the crystallization of PTT and PP components in blends, respectively. The result suggests that both PTT and PP components crystallized individually. By careful observation, it is easy to find that both T_{cI} and T_{cII} values in B0 blends without a compatibilizer are larger than that of B5 and B6, respectively. The changes of T_c values of B0 blend show that crystallizations in PTT and PP phases are improved by the presence of the other component, implying that each component exerts a nucleating effect in the other component's crystallization process and lowers the nucleation energy. Generally, for a two crystallizable component blend, the presence of one component can influence the other's crystallization in three ways. The first is the nucleation effect which lowers the nucleation energy is enhanced by an increase in the interfacial area. The second is the influence on nuclei growth by diluting the concentration of the crystallizable component near the growth fronts. The third is the interference of the component chain segments incorporating into the growing crystal lattice, which increases the system's overall free energy. PTT and PP component are incompatible in PTT/PP blends. The first effect is likely to have greater influences on their crystallization behavior than the second and third effects.

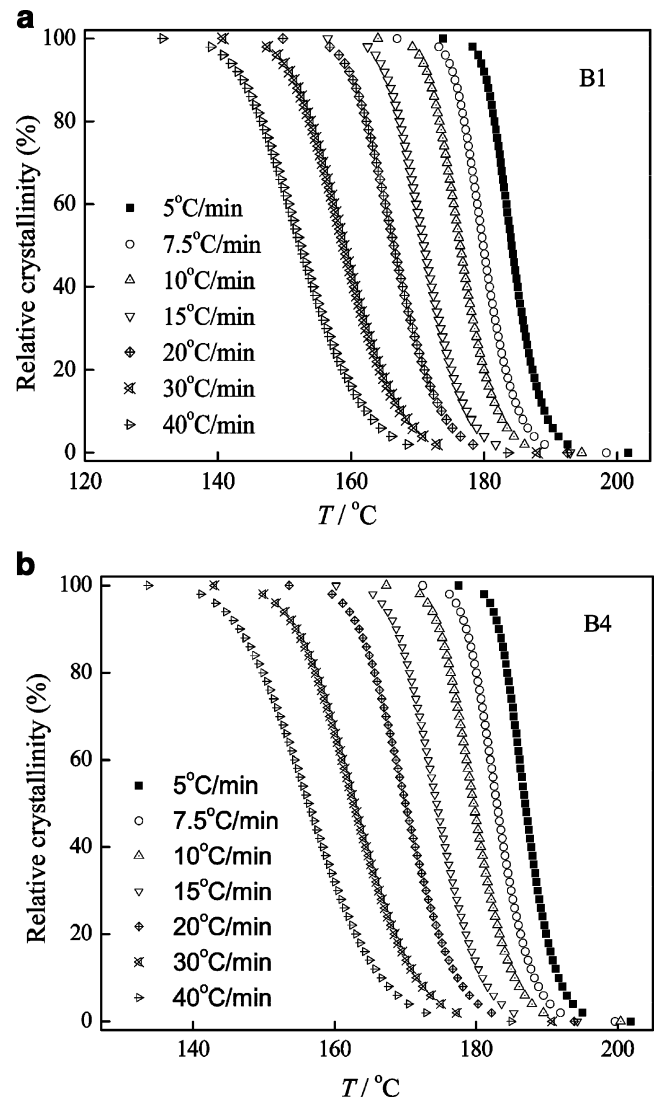


Fig. 4 Relative crystallinity vs. temperature for non-isothermal crystallization of PTT component of **a** B1 and **b** B4 blends

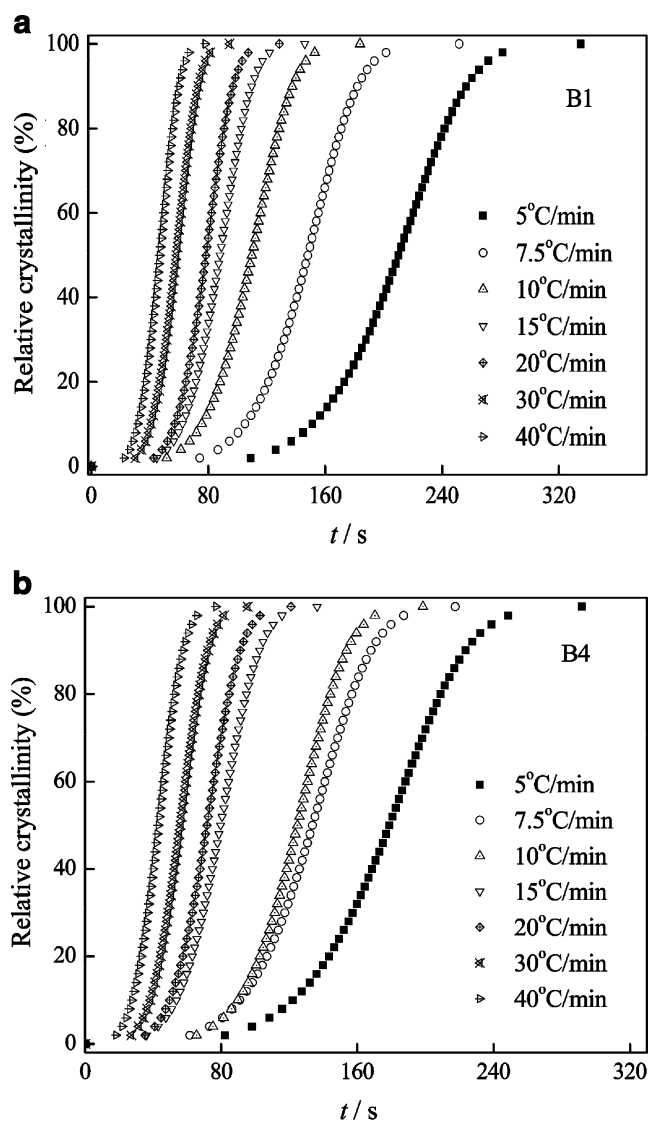


Fig. 5 Relative crystallinity vs. time for non-isothermal crystallization of PTT component of **a** B1 and **b** B4 blends

The DSC curves of B1, B2, B3 and B4 show the effect of adding PP-g-MAH reactive compatibilizer on the crystallization behavior of PTT/PP blends. Compared the crystallization behavior of B1, B2, B3, and B4 blends with that of B0 blend, T_c values of PP component in PTT/PP/PP-g-MAH blends shift significantly to lower temperatures with increasing of the content of the reactive compatibilizer PP-g-MAH, the results suggest that a more intimate interaction formed between PTT and PP-g-MAH, and that may be attribute to the reactions between PP-g-MAH and PTT's hydroxyl endgroups. Consequently, the crystallization of PP component in the compatibilized blends is retarded and its T_c shift to lower temperatures. However, with increasing PP-g-MAH loading, the T_{cII} values increase gradually from 176.9 °C for B1 to 184.0 °C for B4, suggesting that the nucleation effect of PP-g-MAH shows a

greater influence on the crystallization behavior of PTT component. Additionally, the crystallization enthalpies ΔH_c of PTT component decrease gradually from -43.8 to -28.1 J g $^{-1}$, and that of PP component increase gradually from -16.8 to -36.5 J g $^{-1}$ with increasing of the amount of PP-g-MAH from 0% to 30%.

Figure 2 shows a series of DSC thermograms of seven samples at a heating rate of 10 °C/min and the parameters are listed in Table 1. It is clearly seen that the subsequent melting thermograms for B5 (PP) and B6 (PTT) samples exhibit a single endothermic peak with the values of T_m at 161.7 and 225.0 °C, respectively. For the DSC curves from B0 to B4 blends, two endothermic peaks, T_{mI} , at lower temperature and T_{mII} , at higher temperature are found, which corresponds to the melting of the crystals of PP and PTT components, respectively. By careful observation, it is easy to find that the values of melting peak of PTT

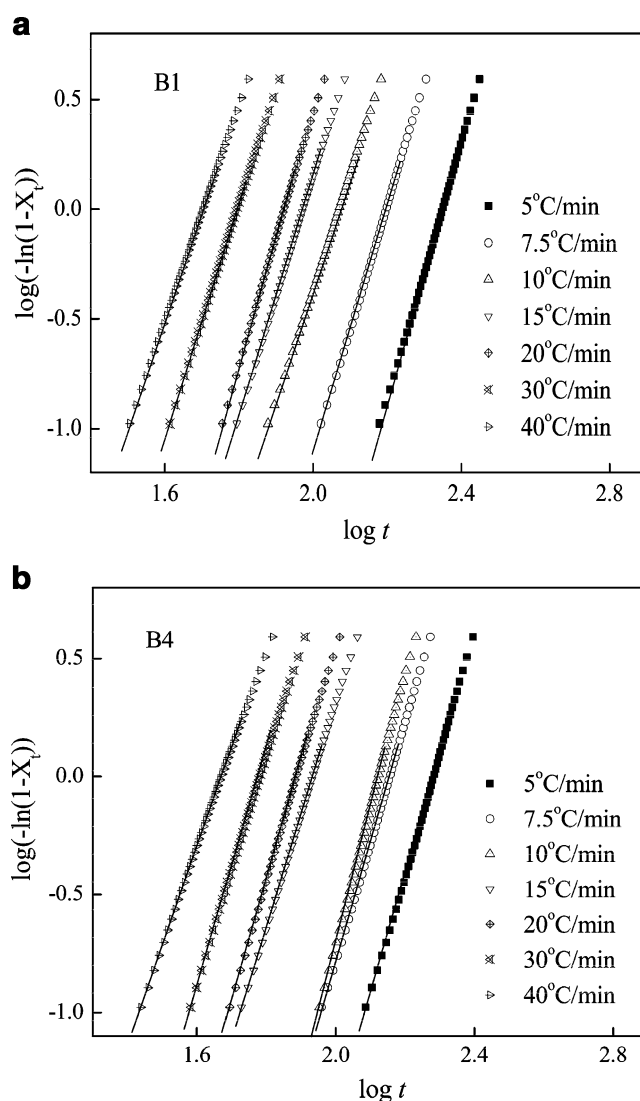


Fig. 6 Plots of $\log[-\ln(1-X_t)]$ vs. $\log t$ for non-isothermal crystallization of PTT component of **a** B1 and **b** B4 blends

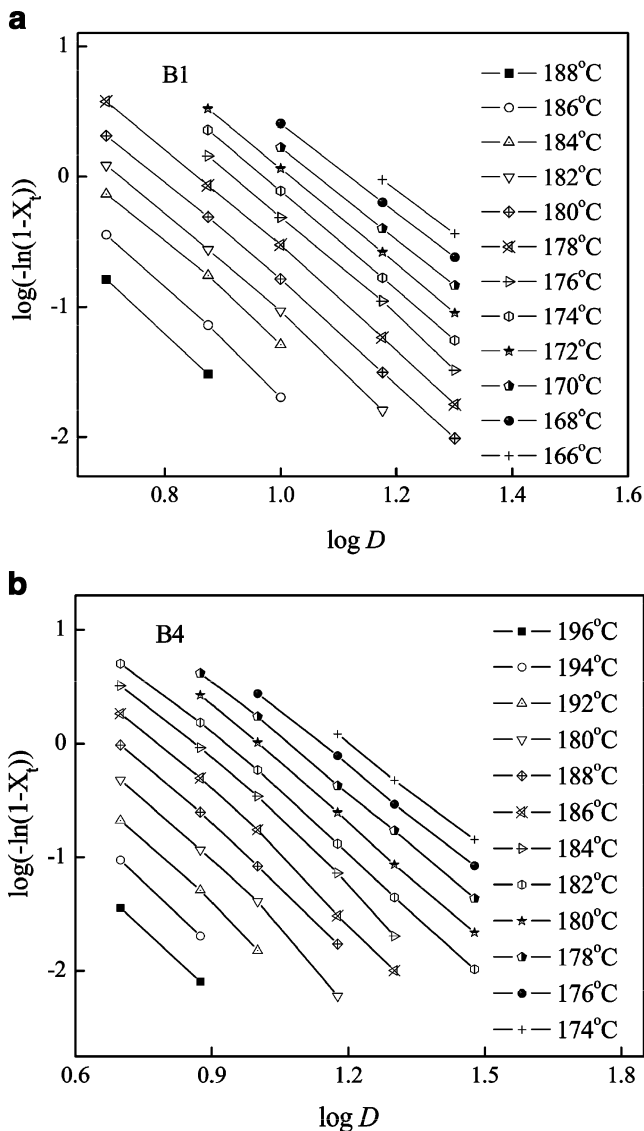


Fig. 7 Ozawa plots of $\log[-\ln(1-X_t)]$ vs. $\log D$ for PTT component of **a** B1 and **b** B4 blends

component decrease from 230.6 to 228.0 °C and that of PP component decreases from 167.6 to 163.8 °C with increasing of the PP-g-MAH loading from 0% (B0) to 30% (B4) blends, which suggesting the crystallinity formed in the process of cooling tends to be more imperfect and trivial.

Non-isothermal crystallization kinetics analysis

Non-isothermal crystallization kinetics analysis of PTT component

Analysis based on the Avrami theory modified by Jeziorny for PTT component In this study, the samples of B1 and B4 are selected to study their non-isothermal crystallization kinetics. The non-isothermal crystallization exothermic

peaks of B1 and B4 blends at various cooling rate, D , are shown in Fig. 3. The parameters of non-isothermal crystallization are summarized in Table 2. All of the exothermic exhibits two crystallization peaks and the values of the exothermic peak temperature, T_{cI} and T_{cII} shift to lower temperature region with increasing of the cooling rates.

From the DSC digital information, the relative crystallinity (X_t) of PTT component are calculated at different temperature T , and the plots of X_t versus T are shown in Fig. 4a (B1) and b (B4). According to Eq. 3 the horizontal T -axis in Fig. 4a, b can be transformed into the crystallization time t -axis as shown in Fig. 5a (B1) and b (B4). The parameters of non-isothermal crystallization are summarized in Table 2.

It can be seen from Fig. 4 that all these curves have similar sigmoidal shape with a fast primary crystallization during the early stage and a slow secondary crystallization at the later stage. The curvature of the upper parts of the plot is observed to be level off due to the spherulites impingement that already begin from the inflection point of the curves. The characteristic sigmoidal curves shift to lower temperature or shorter time with increasing cooling rate. Through Fig. 5a, b, we can get the half time of crystallization, $t_{1/2}$, when the X_t are equal to 50%, and the parameters are listed in Table 2. It can be seen that $t_{1/2}$ values decrease gradually with increasing cooling rates, indicating a progressively faster crystallization rate as the cooling rate increased. Moreover, comparing the values of $t_{1/2}$ of B1 with those of B4 at a given cooling rate, it is clearly that the sample with more the PP-g-MAH component has a lower $t_{1/2}$ values and it take shorter times to reach a given crystallinity. The result suggests that the PP-

Table 3 Non-isothermal crystallization kinetic parameters analyzed by Ozawa equation for PTT component of B1 and B4 blends

B1			B4		
$T/^\circ\text{C}$	m	$\log K(T)$	$T/^\circ\text{C}$	m	$\log K(T)$
188	4.12	2.10	196	3.67	1.12
186	4.12	2.45	194	3.80	1.63
184	3.82	2.55	192	3.78	1.98
182	3.93	2.86	190	3.96	2.50
180	3.88	3.06	188	3.68	2.58
178	3.86	3.30	186	3.81	2.98
176	3.83	3.52	184	3.65	3.12
174	3.79	3.67	182	3.50	3.22
172	3.67	3.74	180	3.48	3.48
170	3.52	3.74	178	3.29	3.51
168	3.41	3.82	176	3.18	3.62
166	3.32	3.90	174	3.06	3.67

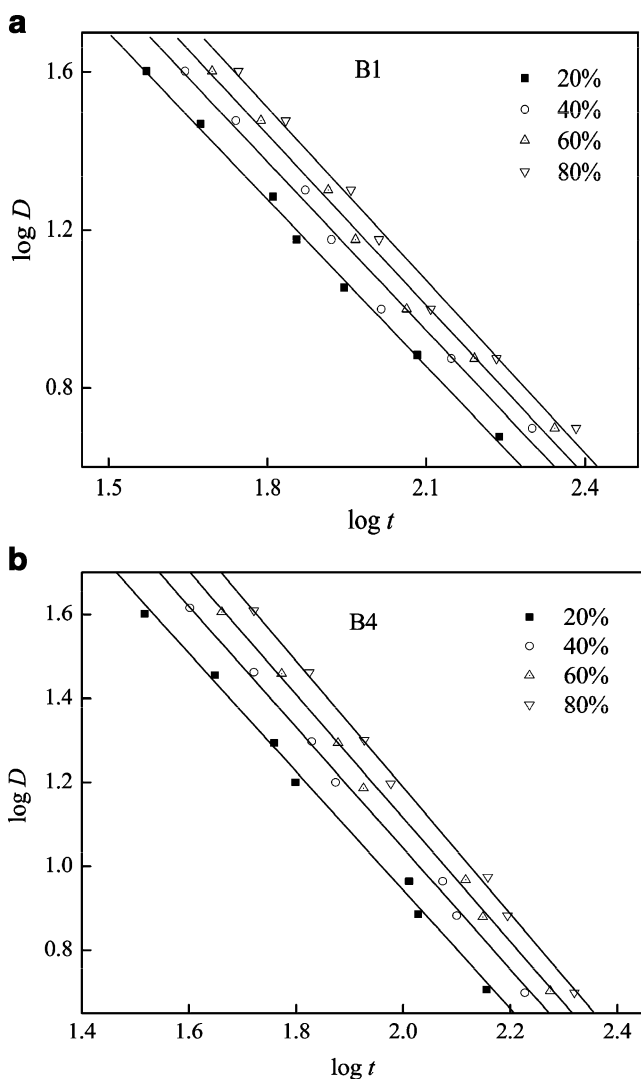


Fig. 8 Log D vs. $\log t$ from the Mo equation for PTT component of **a** B1 and **b** B4 blends

g-MAH component acting a nucleating agent improve the crystallization rate of the PTT component.

Figure 6a, b show a series of double logarithm plot of $\log[-\ln(1-X_t)]$ vs. $\log t$ at different cooling rates. The Avrami exponent n and $\log Z_c$ of B1 and B4 obtained from

Table 4 Non-isothermal crystallization kinetic parameters analyzed by Mo equation for PTT component of B1 and B4 blend at given relative crystallinity

$X_t/\%$	B1		B4	
	b	$\log F(T)$	b	$\log F(T)$
20	1.41	3.78	1.41	3.80
40	1.44	3.93	1.42	3.93
60	1.47	4.04	1.44	4.05
80	1.50	4.18	1.49	4.20

the slopes and the intercepts are also listed in Table 2. Each of curves in Fig. 6 show good linearity.

The Avrami exponent n of the PTT component are found to decrease from 5.9 to 4.9 for B1 and 5.7 to 4.7 for B4 when cooling rate increased from 5 to 40 °C/min, suggesting that the nucleation mechanism changes from a thermal to an athermal mode, with a three-dimensional. It is known that the nucleation mode is dependent on the cooling rate [35]. The values of exponent $n > 4$ at various cooling rates may due to the spherulite's impingement and crowding, or the complicated nucleation types and growth form of spherulites [36]. As shown in Table 2, the values of n decrease gradually for each blend with increasing cooling rate, which indicating the crystallization growth is on fewer dimensions with increasing of the cooling rate, and the spherical crystals turn to be more imperfect. The values of the $\log Z_c$ increase gradually with increasing of the cooling rate. It is well known that the higher cooling rates will result in lower T_p , which in turn results in higher supercooling. Thus, crystallization rates are enhanced. The sample with more PP-g-MAH content (B4) has a higher value of $\log Z_c$ than that with less one (B1) at a given cooling rate, which is consistent with the result of $t_{1/2}$ values. Furthermore, ΔH is gradually decreased due to the forming of imperfect crystalline in the blend with increasing of cooling rate.

Analysis based on the Ozawa theory The result of the Ozawa analysis for B1 and B4 blends are shown in Fig. 7a, b, respectively, and a series of straight lines are obtained. The values of m and $\log K(T)$ are listed in Table 3. For both B1 and B4 blends, the values of m are increased with increasing of temperature, indicating the crystallization growth is on

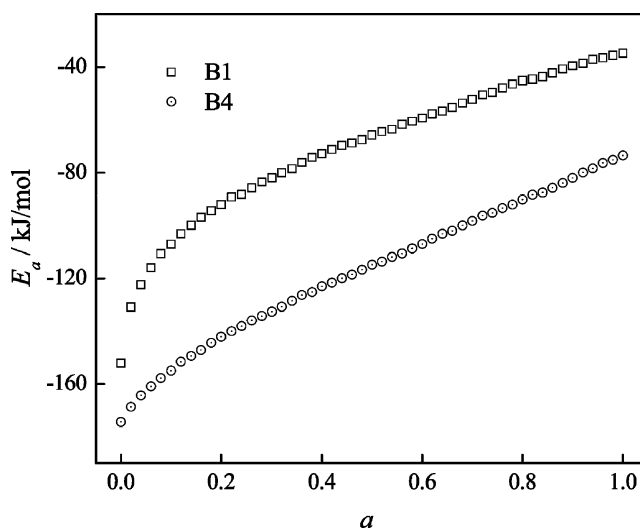


Fig. 9 Dependence of the effective activation energy of PTT component of B1 and B4 blends on the relative extent of crystallization

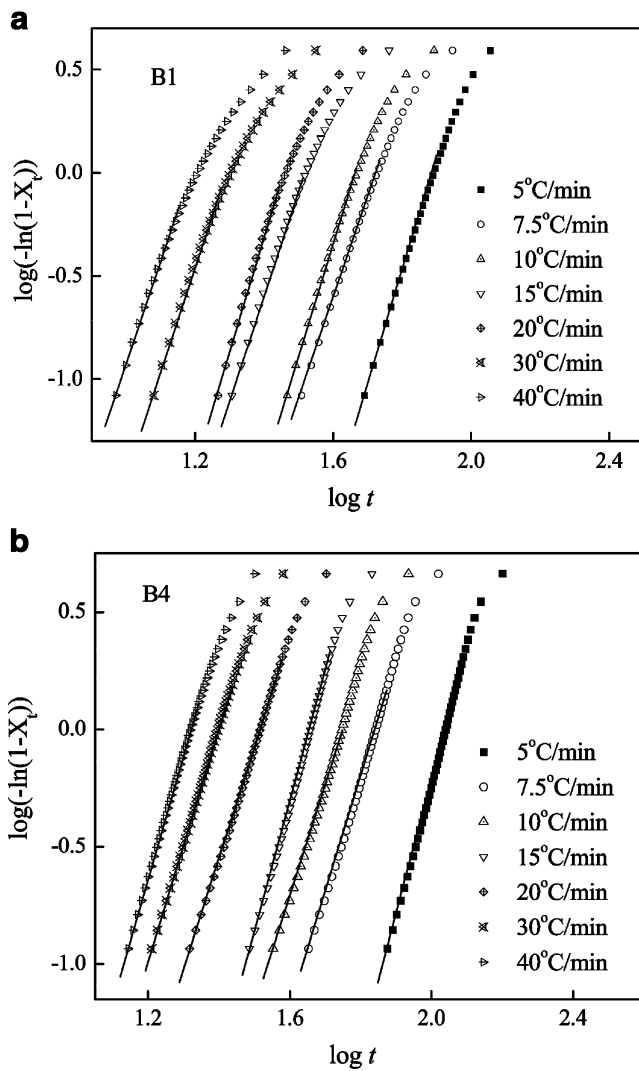


Fig. 10 Plots of $\log[-\ln(1-X_t)]$ vs. $\log t$ for non-isothermal crystallization of PP component of **a** B1 and **b** B4 blends

more dimensions at higher temperature, while it is on fewer dimensions at lower temperature. The values of $\log K(T)$ decrease gradually from 3.90 to 2.10 with temperature increasing from 166 to 188 °C for B1 blend, and from 3.67 to 1.12 with increasing temperature from 174 to 196 °C for B4 blend, which suggests that the crystallization rate is faster at lower temperature than that at higher temperature. Moreover, the values of $\log K(T)$ of B4 is larger than that of B1 blend at same temperature range of 174 to 188 °C, indicating the introduction of PP-g-MAH in the blends improve the crystallization rate of PTT component, which is also conformed by the results of Avrami analysis. Therefore, an accurate analysis of PTT component for B1 and B4 blends of non-isothermal crystallization data could be performed with Ozawa theory.

Analysis based on the Mo theory As shown in Fig. 8, plotting $\log D$ against $\log t$ for B1 and B4 blends demonstrates linear relationship at a given X_t , and the values of $\log F(T)$ and b are listed in Table 4. $\log F(T)$ values increases with the relative crystallinity from 3.78 to 4.18 for B1 and 3.80 to 4.20 for B4. The parameters b shows only a little increase with increasing X_t , ranging from 1.41 to 1.50 for B1 and 1.41 to 1.49 for B4, respectively. Compared the values of $\log F(T)$ of B1 with those of B4 at a given X_t , it is obviously that the results of B1 are less than those of B4, indicating that the more the PP-g-MAH content, the higher the crystallization rate is. This conclusion is confirmed by the results of Avrami and Ozawa theory. Thus, the equation of Mo method also successfully describes the non-isothermal crystallization process of PTT component in the binary blends on the whole crystallization process.

Crystallization activation energy Because it has to release energy when the molten fluid transformed into the

Table 5 Parameters of non-isothermal crystallization analyzed by Avrami theory for PP component of B1 and B4 blends

Samples	$D/^\circ\text{C min}^{-1}$	$T_m/^\circ\text{C}$	$t_{1/2}/\text{s}$	n	$\log Z_f/s^{-n}$	$\log Z_c/s^{-n}$	$\Delta H/\text{J g}^{-1}$
B1	5	124.4	72.5	5.4	-10.28	-2.06	-18.38
	7.5	122.5	49.3	5.0	-8.64	-1.15	-18.33
	10	121.1	43.1	5.5	-9.11	-0.91	-18.35
	15	118.9	30.5	5.2	-7.90	-0.53	-18.20
	20	117.2	26.7	5.8	-8.34	-0.42	-18.24
	30	114.3	18.3	5.1	-6.54	-0.22	-17.97
	40	111.9	14.6	4.8	-5.72	-0.14	-17.87
B4	5	120.9	103.3	5.7	-11.66	-2.3	-37.13
	7.5	118.9	65.0	4.9	-9.08	-1.21	-36.57
	10	117.1	52.1	4.8	-8.47	-0.85	-36.42
	15	114.8	42.8	5.4	-9.04	-0.60	-36.01
	20	112.9	30.5	4.7	-7.20	-0.36	-35.47
	30	110.1	23.2	5.0	-7.03	-0.23	-34.56
	40	107.9	19.5	5.2	-6.98	-0.17	-33.98

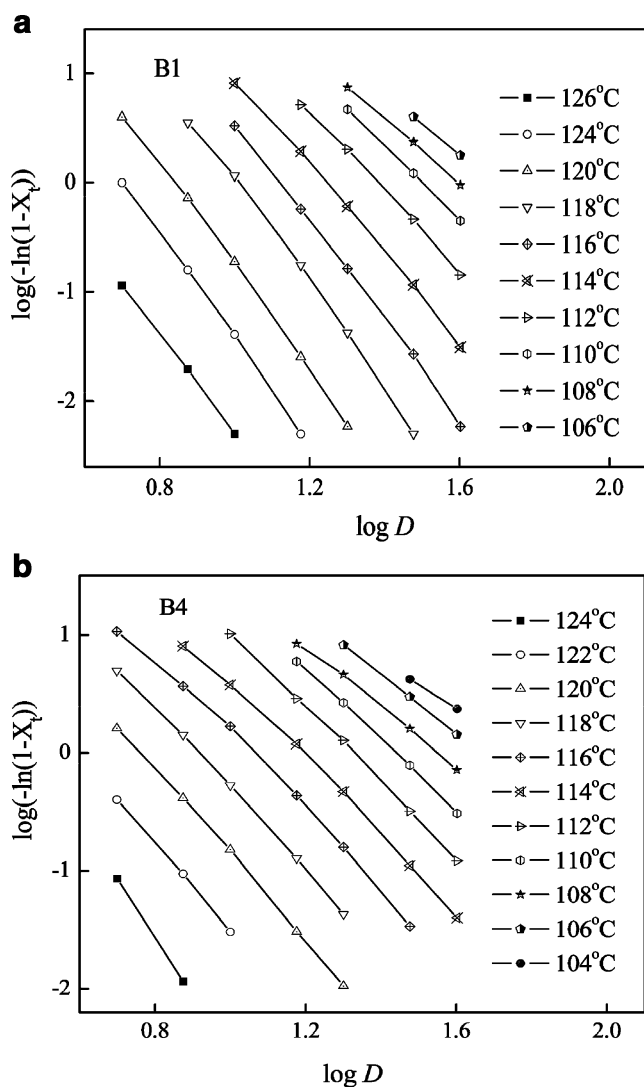


Fig. 11 Ozawa plots of $\log[-\ln(1-X_t)]$ vs. $\log D$ for PP component of **a** B1 and **b** B4 blends

Table 6 Non-isothermal crystallization kinetic parameters analyzed by Ozawa equation for PP component of B1 and B4 blends

B1			B4		
$T/^\circ\text{C}$	m	$\log K(T)$	$T/^\circ\text{C}$	m	$\log K(T)$
126	4.50	2.21	124	4.95	2.18
124	4.79	2.49	122	3.71	2.20
122	4.81	3.39	120	3.65	2.79
120	4.72	3.95	118	3.43	3.13
118	4.74	4.77	116	3.21	3.36
116	4.21	4.97	114	3.18	3.76
114	4.08	5.02	112	3.19	4.22
112	3.65	5.03	110	3.02	4.34
110	3.38	5.08	108	2.53	3.93
108	3.02	4.81	106	2.53	4.21
106	2.81	4.75	104	2.00	3.58

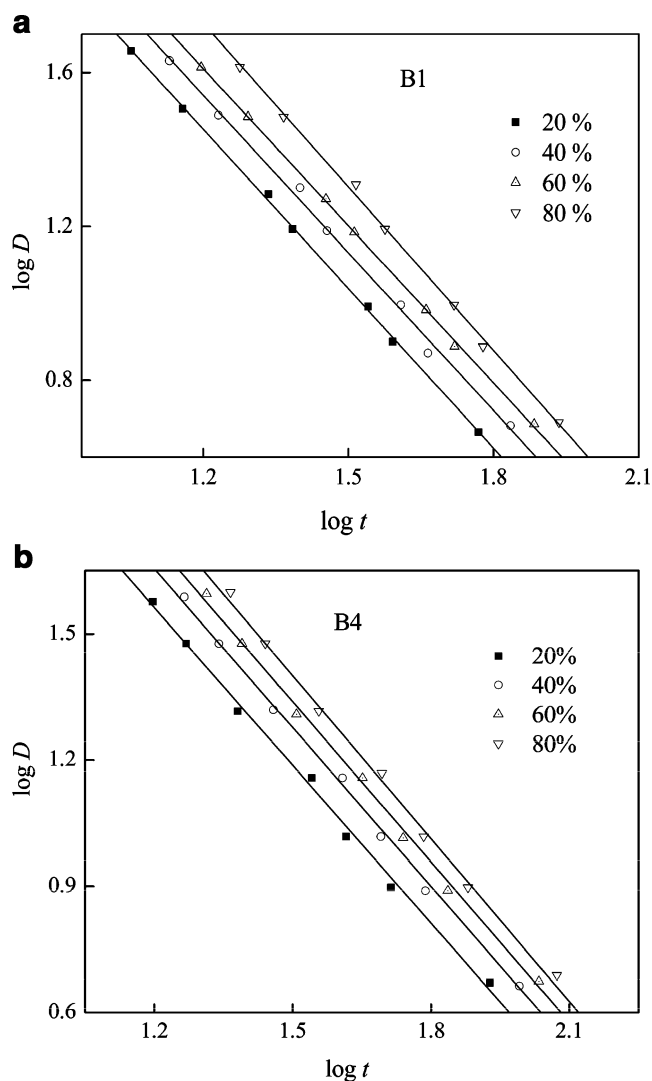


Fig. 12 $\log D$ vs. $\log t$ from the Mo equation for PP component of **a** B1 and **b** B4 blends

crystalline state, the value of ΔE is negative on the basis of the concept of the heat quantity in physical chemistry. In this study, as shown in Fig. 9, the ΔE_a values of PTT component increase from -152.2 to -34.8 kJ mol^{-1} for B1 and from -174.2 to -72.7 kJ mol^{-1} for B4 with increasing relative crystallinity, respectively. This result suggests that

Table 7 Non-isothermal crystallization kinetic parameter analyzed by Mo equation for PP component of B1 and B4 blends

$X_t/\%$	B1		B4	
	b	$\log F(T)$	b	$\log F(T)$
20	1.36	3.11	1.25	3.06
40	1.37	3.18	1.26	3.16
60	1.36	3.25	1.27	3.24
80	1.42	3.43	1.29	3.34

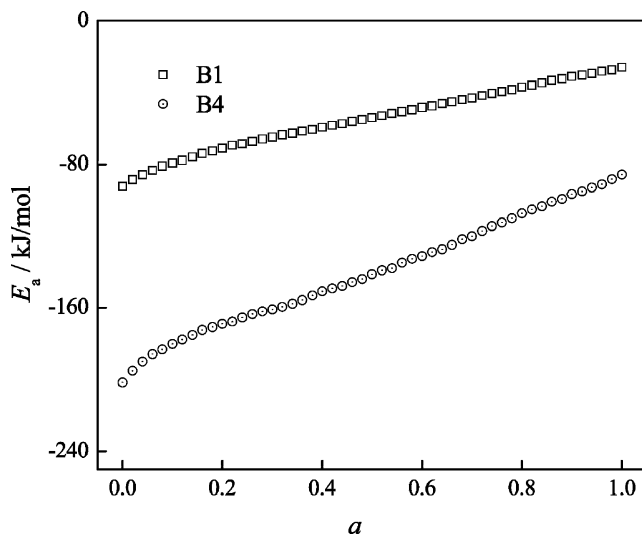


Fig. 13 Dependence of the effective activation energy of PP component of B1 and B4 blends on the relative extent of crystallization

the crystallization become easier as the crystallization proceed. Moreover, the PTT component of B1 blend has the higher crystallization ability than that of B4 blend, which is consent with the result above-mentioned.

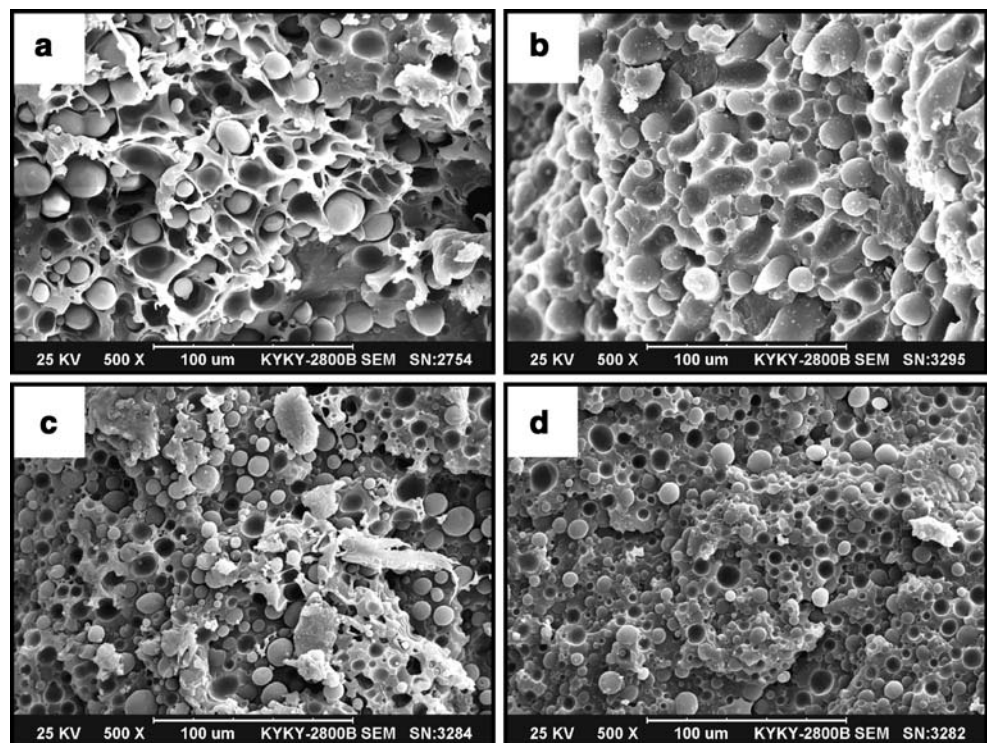
Non-isothermal crystallization kinetics analysis of PP component

Analysis based on the Avrami theory modified by Jeziorny for PP component Figure 10a, b show a series of double

logarithm plot of $\log[-\ln(1-X_t)]$ vs. $\log t$ of PP component at different cooling rates. The kinetics parameters are listed in Table 5. Each of curves in Fig. 10 shows good linearity except a secondary crystallization at the later crystallization stage. The Avrami exponent n of the PP component is found to range from 5.4 to 4.8 for B1, and 5.4 to 4.7 for B4 when cooling rate increased from 5 to 40 °C/min. The half time of crystallization $t_{1/2}$ values decrease from 72.5 to 14.6 s for B1 and from 103.3 to 19.5 s for B4 with increasing cooling rates. Comparing the values of $t_{1/2}$ of PP component of B1 with those of B4 at a given cooling rate, it is clearly that the more the PP-g-MAH component in blends, the higher the $t_{1/2}$, namely, the lower the crystallization rate of PP component is. ΔH gradually decreases due to the less perfect crystallites formed in the blend with increasing cooling rate. Moreover, the values of $\log Z_c$ of B1 are larger than those of B4 at a given cooling rate, which suggest the blend with more PP-g-MAH content has a lower crystallization rate than the less one, and which is approved with the result of $t_{1/2}$.

Analysis based on the Ozawa theory The result of the Ozawa analysis for PP component of B1 and B4 blends are shown in Fig. 11a, b, where the values of m and $\log K(T)$ are listed in Table 6. The values of m increased from 2.81 to 4.81 with increasing temperature from 106 to 126 °C for B1 blend, and from 2.00 to 4.95 for B4 blend with the increasing temperature from 104 to 124 °C for B4, which indicates that the crystallization growth of PP component is

Fig. 14 SEM photographs of crisp fracture surface of blends a B0, b B1, c B2 and d B3



on more dimensions at a higher temperature and on fewer dimensions at lower temperature. The values of parameters $\log K(T)$ decrease from 5.08 to 2.21 for B1 and from 4.34 to 2.18 for B4 blends, which suggests that the crystallization rate is faster at lower temperature than that at higher temperature. Comparing the values of $\log K(T)$ of B1 with those of B4 at the same temperature range of 106 to 124 °C, it is obviously that the results of B4 is lower than those of B1, which indicating the introduction of PP-g-MAH component decreases the crystallization rate of PP component.

Analysis based on the Mo theory Figure 12 shows the results analyzed according to Mo's method, and the parameters of $\log F(T)$ and b are listed in Table 7. $\log F(T)$ values increased from 3.11 to 3.43 for B1 and from 3.06 to 3.34 for B4 with increasing the relative crystallinity, indicating a lower crystallization rate is needed to reach the given crystallinity within unit time. The parameters b increase from 1.36 to 1.42 for B1 and from 1.25 to 1.29 for B4 with increasing X_c , respectively. Comparing the values of b and $\log F(T)$ of B1 with those of B4 at a given X_c , one can find that the results of B1 are higher than those of B4, which suggesting the crystals growth is on more dimensions and fast crystallization rate with the lower PP-g-MAH content. The equation of Mo method can also described the non-isothermal crystallization process of the binary blends successfully.

Crystallization activation energy The results of Vyazovkin analysis for PP component of B1 and B4 blends are shown in Fig. 13. And the ΔE_a values are found to increase from -92.3 to -25.7 kJ g⁻¹ for B1 blend and from -201.5 to -84.9 kJ g⁻¹ for B4 blend with increasing of relative crystallinity. This result suggests that it is difficult for blends to crystallize at the beginning of the crystallization, while it becomes easy as the crystallization proceed. Furthermore, B1 has a lower effective energy barrier than B4. Consequently, the PP component of the blend with less PP-g-MAH component has the higher crystallization ability than that with more PP-g-MAH content.

The morphology of the PTT/PP-g-MAH/PP blends

The PTT and PP are not miscible because they have a large difference in their solubility parameters. However, the PP-g-MAH acts as a compatibilizer for PTT/PP blend to improve and stabilize the morphological structure, through the reaction between the maleated anhydride moiety and PTT's hydroxyl endgroup during melt blending. The SEM photographs of crisp fracture surface of B0, B1, B2 and B3 blends are displayed in Fig. 14a–d. As shown in Fig. 14a, the blending of PTT and PP displays in a heterophase system with PTT as the continuous phase and PP as

particles. The minor phase of PP is coarsely dispersed in the continuous PTT matrix in essentially spherical domains. The interface of two phases is loose and obviously separated from each other. As shown in Fig. 14b–d, With increasing the contents of PP-g-MAH, the droplets are quite uniformly distributed inside the PTT matrix, interfacial thickness of PTT/PP blend is improved and the particle size turn to be smaller than that of B0 blend, all of these result suggest that the compatibility of PTT with PP is markedly improved. This shows that the PP-g-MAH as an effective compatibilizer decreases the interfacial tension and increases the adhesion phases of the blend as expected.

Conclusions

PTT/PP-g-MAH/PP blends prepared by melt-compound are investigated by using differential scanning calorimeter (DSC). The results demonstrate different crystallization and melting behaviors with varied content of PP-g-MAH in blends. All of the three methods including Avrami equation modified by Jeziorny, Ozawa and Mo have successfully simulated the primary stage of non-isothermal crystallization process of PTT and PP component. The crystallization of PTT component is accelerated, however, that of PP component is retarded by the introduction of PP-g-MAH. The effective activity energy calculated by Vyazovkin method suggests that both PP and PTT component of the blend B1 has higher crystallization ability than those of B4. Moreover, PP-g-MAH as an effective compatibilizer decreases the interfacial tension and increases the compatibility of the blend.

Acknowledgment The work is supported by the financial support from the Natural Science Foundation of Hebei Province (B2007000108), PR China.

Reference

- Whinfield JR, Dickson JT (1946) Brit Pat 578:079
- Wu J, Schultz JM, Samon JM et al (2001) Polymer (Guildf) 42:7141. doi:10.1016/S0032-3861(01)00042-8
- Grande JA (1997) Mod Plast 12:97
- Li JX, Cheung WL, Jia D (1999) Polymer (Guildf) 40:1219. doi:10.1016/S0032-3861(98)00345-0
- Coccorullo I, Pantani R, Titomanlio G (2003) Polymer (Guildf) 44:307. doi:10.1016/S0032-3861(02)00762-0
- Masubuchi Y, Watanabe K, Nagatake W et al (2001) Polymer (Guildf) 42:5023. doi:10.1016/S0032-3861(00)00886-7
- Assoulinea E, Pohl S, Fulchiron R et al (2000) Polymer (Guildf) 41:7843. doi:10.1016/S0032-3861(00)00113-0
- Supaphol P, Lin JS (2001) Polymer (Guildf) 42:9617. doi:10.1016/S0032-3861(01)00507-9
- Supaphol P, Spruiellb JE (2001) Polymer (Guildf) 42:699. doi:10.1016/S0032-3861(00)00399-2

10. Zhang Y, Jiang X, Guan Y et al (2005) *Mater Lett* 59:3626. doi:10.1016/j.matlet.2005.07.010
11. Supaphol P (2001) *Thermochim Acta* 370:37. doi:10.1016/S0040-6031(00)00767-X
12. Sekia M, Yamauchia S, Matsushita Y (1999) *J Phys Chem Solids* 60:1333. doi:10.1016/S0022-3697(99)00120-1
13. Silvestre C, Cimmino S, Alma ED et al (1999) *Polymer (Guildf)* 40:5119. doi:10.1016/S0032-3861(98)00696-X
14. Shieh YT, Lee MS, Chen SA (2001) *Polymer (Guildf)* 42:4439. doi:10.1016/S0032-3861(00)00567-X
15. Rabello MS, White JR (1997) *Polymer (Guildf)* 38:6389. doi:10.1016/S0032-3861(97)00214-0
16. Albano C, Papa J, Ichazo M et al (2003) *Compos Struct* 62:291. doi:10.1016/j.compstruct.2003.09.028
17. Campoy I, Arribas JM, Zaporta MAM et al (1995) *Eur Polym J* 31:475. doi:10.1016/0014-3057(94)00185-5
18. Chen JH, Tsai FC, Nien YH et al (2005) *Polymer (Guildf)* 46:5680. doi:10.1016/j.polymer.2005.03.107
19. Xiao Z, Li L, Zhou D et al (2003) *Thermochim Acta* 404:283. doi:10.1016/S0040-6031(03)00186-2
20. Hieber CA (1995) *Polymer (Guildf)* 36:1455. doi:10.1016/0032-3861(95)95925-Q
21. Dangseeeyun N, Supaphol P, Nithitanakul M (2004) *Polym Test* 23:187. doi:10.1016/S0142-9418(03)00079-5
22. Rwei SP (1999) *Polym Eng Sci* 39:2475
23. Ravikumar HB, Ranganathaiah C, kunavaswamy GN et al (2005) *Polymer* 46:2372. doi:10.1016/j.polymer.2004.12.058
24. Zhang QX, Yu ZZ, Xie XL et al (2004) *Polymer (Guildf)* 45:5985. doi:10.1016/j.polymer.2004.06.044
25. Chan CM, Wu JS, Li JX et al (2002) *Polymer (Guildf)* 43:2981. doi:10.1016/S0032-3861(02)00120-9
26. Xu WB, Liang GD, Zhai HB et al (2003) *Eur Polym J* 39:1467. doi:10.1016/S0014-3057(03)00015-6
27. Xue ML, Yu YL, Chuah HH (2007) *J Macromol Sci Phys* 46:603. doi:10.1080/00222340701258008
28. Avrami M (1940) *J Chem Phys* 8:212. doi:10.1063/1.1750631
29. Jeziorny A (1978) *Polymer (Guildf)* 19:1142. doi:10.1016/0032-3861(78)90060-5
30. Ozawa T (1971) *Polymer (Guildf)* 12:150. doi:10.1016/0032-3861(71)90041-3
31. Liu TX, Mo ZS, Zhang HF (1998) *J Polym Eng* 18:283
32. Friedman H (1964–1965) *J Polym Sci* 6(Part C):183
33. Vyazovkin S (1997) *J Comput Chem* 18:393. doi:10.1002/(SICI)1096-987X(199702)18:3<393::AID-JCC9>3.0.CO;2-P
34. Vyazovkin S (2001) *J Comput Chem* 22:178. doi:10.1002/1096-987X(20010130)22:2<178::AID-JCC5>3.0.CO;2-#
35. Choe CR, Lee KH (1989) *Polym. Eng Sci* 29:801
36. Liu MY, Zhao QX, Wang YD et al (2003) *Polymer (Guildf)* 44:2537. doi:10.1016/S0032-3861(03)00101-0